Towards 3D Raman Sideband Cooling of Rubidium

von

Amirhosein Mohammadi Moqanaki

Masterarbeit in Physik

angefertigt im

Institut für Angewandte Physik

vorgelegt der

Mathematisch-Naturwissenschaftlichen Fakultät der Universität Bonn

November 2010

Declaration of Authorship

I, Amirhosein Mohammadi Moqanaki, hereby certify that the work presented here was accomplished by myself and without the use of illegitimate means or support, and that no sources and tools were used other than those cited.

Signed:

_____

Date:

_____

1. Gutachter: Prof. Dr. Dieter Meschede

2. Gutachter: Prof. Dr. Marek Kowalski

"Birthdays are good for you. Statistics show that the people who have the most live the longest."

Larry Lorenzoni

RHEINISCHE FRIEDRICH-WILHELMS-UNIVERSITÄT BONN

Abstract

Institut für Angewandte Physik

Mathematisch-Naturwissenschaftlichen Fakultät der Universität Bonn

Masterarbeit in Physik

by Amirhosein Mohammadi Moqanaki

Raman sideband cooling is a method to prepare atoms in the vibrational ground state of a periodic potential and cool them below recoil limit. It can be implemented as a mid-stage cooling to improve the efficiency and speed of evaporative cooling. The aim of this text is introducing its principle, design of such an apparatus for Rubidium atoms using diode lasers and explain technical details of set up process.

Acknowledgements

Contents

List of Figures

Abbreviations

MOT	**M**agneto **O**ptical **T**rap
OM	**O**ptical **M**olasses
BEC	**B**ose **E**instein **C**ondensate
FORL	**F**ar **O**ff **R**esonance **L**attice
UHV	**U**ltra **H**igh **V**acuum
ECDL	**E**xternal **C**avity **D**iode **L**aser
AOM	**A**cousto **O**ptical **M**odulator
RGA	**R**esidual **G**as **A**nalyzer
AR	**A**nti **R**eflective
SMD	**S**urface **M**ount **D**evice
RF	**R**adio **F**requency

Chapter 1

Introduction

Bose-Einstein Condensate (BEC) is a pure quantum mechanical system, a state of matter of a dilute gas of weakly interacting bosons. It appears in temperatures very close to the absolute zero (nano Kelvin regime) [8, 24].

In 1995 the first Bose-Einstein Condensate (BEC) samples were produced [7, 9, 21] shown in the Table. 1.1.

The BEC transition occurs after cooling down the matter below a critical temperature or more precisely when *phase space density* $(n\lambda_d^3 B)$ reaches 2.612 [8, 24] (for comparison see Table. 1.2).

	JILA	Rice	MIT
Group	Wieman-Cornell	Hulet	Ketterle
Place	Colorado	Houston	Boston
Atom	Rb	Li	Na
Cooling	MOT	Doppler slowing	Zeeman slowing
Trap	TOP	Permanent magnetic trap	Magnetic trap with optical plug
First BEC	June 95	July 95	Sept. 95
T_C μK	0.1	0.4	2
N	2×10^4	2×10^5	2×10^6
n_C (cm^{-3})	2×10^{12}	2×10^{12}	1.5×10^{14}
τ (s)	15	20	1

TABLE 1.1: Comparison between first three reported BEC experiments [36].

Stages	T	n (cm^{-3})	nλ_{dB}^3
Oven	573 K	10^{10}	10^{-17}
Slowing	30 mK	10^8	10^{-12}
Cooling	1 mK	10^9	10^{-9}
Trapping	1 mK	10^{12}	10^{-6}
Evaporation	70 nK	10^{12}	2.612

TABLE 1.2: Typical values for phase space density [36].

To reach such high phase space density for neutral atoms, MOT has become the ubiquitous tool for its robustness and simplicity comparing to the other methods [17]. Combining six counter-propagating laser beams intersecting at one point and a magnetic quadrupole, MOT is built [17, 31]. The laser beams cool the atoms by Doppler cooling [17, 31] and the magnetic quadrupole field provides a trap that keeps the atoms in the intersection of the beams [17, 31]. But life is not as easy as it looks; There are certain limits to pass. In Doppler cooling when the detuning of the laser light is comparable to the natural linewidth the cooling process stops. This limit is called the *Doppler limit* [17].

Doppler limit (at about 300 μK)is many orders of magnitude above the BEC transition but Doppler limit is not the main barrier. In fact laser cooling has worked better than people have predicted and on very early days of implementation of laser cooling, passing Doppler limit has been reported [10, 11]. The more challenging limit is the temperature corresponding to a single photon recoil, referred to as the *recoil limit* [17]. As recoil limit implies we can not remove momentum from an atom less than a quanta (single photon's kick) in a resonat light field but still further cooling is possible [17].

To bypass the recoil limit (at about 3 μK) and reach the BEC transition *evaporative cooling* [22] is the final cooling stage to reach BEC transition. Evaporative cooling is the known everyday phenomena of cooling down of a hot meal or shivering after coming out of the swimming pool. In a simple picture, evaporative cooling works by trapping atoms and tuning the trapping potential in a proper frequency that lets the hot atoms fly away from the trap. This results a very cold sample. Evaporative cooling takes considerable amount of time (in our BEC experiment about 20 s) and this reduces the temporal resolution of our experiment since we are interested in observing interactions of single Cesium atoms with a Rubidium BEC a higher temporal resolution is of interest. The elastic collision of the atoms defines the evaporative cooling's time, therefore providing a colder sample for

evaporative cooling (that consequently has longer elastic collision time) leads to shorter cooling time.

In the vicinity of recoil limit atoms are incredibly cold but they still have vibrations and rotations. Damping the vibrational states of the atom leads to temperatures below recoil limit. Raman transitions [6] inside an optical lattice is a method to bring the atoms to their vibrational ground states [2]. An optical lattice is a spatially periodic potential (or simply set of standing waves) formed by the interference of counter-propagating beams [19]. By being trapped in an off resonant detuned optical lattice, atoms can be isolated from interacting with resonant scattered photons. That makes passing recoil limit possible [34].

A typical Raman sideband cooling can reach phase space densities as high as 0.001 [2, 16, 29], therefore, if it is implemented as a cooling stage before evaporative cooling it can decrease the cooling time to about 2 s.

The aim of this thesis is designing a simple 3D Raman sideband cooling setup for Rubidium using diode lasers. Most of the previous work on Raman sideband cooling is carried out with Cesium [2, 16, 29] and in fact Cesium level scheme is more suitable for Raman sideband cooling [13]. Therefore, I had to adopt the schemes for Cesium and compile them for Rubidium.

In chapter 2, I introduced the principle of Raman sideband cooling and discussed its cooling mechanism. In chapter 3, the design for the apparatus is introduced. It consists of a MOT that traps and pre-cools the atoms and a 3D optical lattice that performs the Raman sideband cooling. The apparatus is designed to wield three external cavity diode lasers for Rubidium 87 D2-line at 780 nm with 40 mW and 60 mW power. A UHV system is necessary as well to provide the environment (dilute atomic Rubidium gas) for the experiment. Building this UHV system covered most of the time I had to do my thesis therefore it is discussed in details: cleaning process, diagnosing its problems and fixing them. Finally in chapter 4 the conclusions and outlook for the apparatus are presented.

Chapter 2

Raman Sideband Cooling

Stimulated Raman transitions [6] inside an optical lattice can change the vibrational states of the atoms trapped inside, thus a deliberately chosen set of polarized laser beams can transfer the atoms to their ground state of motion and overcome the recoil limit [2, 19, 29]. The limits of sideband cooling are determined by heating from off-resonant stimulated Raman transitions and off-resonant spontaneous Raman emissions [27].

2.1   Lamb-Dicke Regime

The optical lattice should provide a tight binding for the atoms, meaning it should keep the atoms safe from the scattered resonant photons and suppress the heating by them [13]. This can be quantified in terms of *Lamb-Dicke parameter* [5, 13]. The Lamb-Dicke parameter (η) gives the ratio of the ground state wave-packet size to the wavelength of the interacting laser light [5]. In an optical lattice it can be interpreted as the ratio of photon recoil energy to the energy separation in the vibrational modes [5, 13] thus

$$\eta = \sqrt{\frac{E_r}{E_v}} < 1 \tag{2.1}$$

In which E_r is recoil energy and E_v vibrational energy. $\eta < 1$ is referred to as *Lamb-Dicke limit.* In this regime clearly vibrational energy is larger than the recoil

energy that means the scattered photons can not change the vibrational state of the atom [13]. For ^{87}Rb we can write down

$$E_r = \frac{\hbar^2\omega_0^2}{2mc^2} = h \cdot 3.8\,kHz \qquad (2.2)$$

Thus the vibrational frequency of the ^{87}Rb atoms inside the lattice should be larger than $3.8kHz$ [13].

On the other hand, the vibrational frequencies should be comparable or larger than the Raman transitions and can be shown that it is in kHz range [13].

Given the vibrational frequency for a sinusoidal optical lattice with depth of E and spatial period L

$$\omega_v = \frac{2}{L}\sqrt{\frac{2E}{m}} \qquad (2.3)$$

Lamb-Dicke limit can be rewritten as

$$L < \sqrt{\frac{8E}{mw_r^2}} \qquad (2.4)$$

For example, for an optical lattice with depth of $40\,\mu K$ the limit is $740\,nm$ which clearly ^{87}Rb D2 line at $780\,nm$ satisfies the condition and gives $\eta = 0.3$ [13].

2.2 Degenerate Raman Sideband Cooling

Degenerate approach to Raman sideband cooling has been demonstrated for the first time in [2].

A proposed cooling cycle for ^{87}Rb based on degenerate Raman sideband cooling [2, 13, 29] is the following: an atom begins initially in the $F = 1, m_F = 1$ ground state in a high-lying vibrational level of the optical lattice (see Fig. 2.1) [2, 13, 29]. To start with this state a separate pump beam can bring the atoms inside the lattice to $F = 1, m_F = 1$ state [2, 13, 29]. A magnetic field is applied to shift the hyperfine levels (m_F states) in a fashion that the Zeeman splitting exactly meets

the spacing of the vibrational levels in the optical lattice [2, 13, 29]. This causes degeneracy in the vibrational levels. Basically, all the sates with the same $\nu - m_F$ become degenerate [13]. Since $F = 1, m_F = 1$ is dark to the resonant light and degenerate with $m_F = 0, \nu - 1$ and $m_F = -1, \nu - 2$ states, proper detuning of the lattice beam can induce Raman transitions and transfer the atom from $m_F = 1$ to $m_F = 0$ and subsequently to $m_F = -1$ and bring the atom to two steps lower vibrational level. [2, 13, 29]. Optical pumping back to $m_F = 1$ preserving the vibrational number, closes the cycle [2, 13, 29]. This is done by pumping the atom to $F = 0, m_F = 0$ and since the optical lattice is in the Lamb-Dicke regime (recall, vibrational energy is larger than the recoil energy), the decay from $F = 0, m_F = 0$ favors $F = 1, m_F = 1$ and does not change the vibrational state [2, 13, 29]. This cycle is repeated until the atom reaches the vibrational ground state in $m_F = 1$ which is dark to both the resonant light and the Raman transitions [2, 13, 29].

Optical pumping back to $m_F = 1$ is done by a pump beam consisting of a strong σ^+ polarized component and a very weak π component, applied on the $F = 1 \longrightarrow F' = 0$ transition [2, 13, 29]. Polarization of this beam has to be carefully adjusted with respect to the magnetic field such that the σ^- component vanishes. Slightly tilting the magnetic field towards the pump beam a weak π component appears. This provides pumping back all the atoms to the $m_F = 1$ since $F = 1, m_F = 0$ is dark to purely σ-polarized light.

This pumping technique suppresses absorption heating in the final cooling stage, and produces lower temperatures than pumping on a transition with pure σ^+ light [2] but there is still a small probability for atoms to end up in $F = 2$ ground state therefore an additional re-pumping beam resonant to $F = 2 \longrightarrow F' = 1$ or $F = 2 \longrightarrow F' = 2$ transitions is needed. Alternatively, this can be done by tuning the lattice beam resonant to one of these transitions [29].

Therefore, a possible Raman sideband cooling recipe has the following steps:

- Loading atoms from the background gas into a MOT.

- Cooling them down and storing them in a far-red-detuned lattice to reduce the scattering from spontaneous emission.

- An external magnetic field (Zeeman shift) or electric field (Stark shift [35]) tunes the vibrational levels spacings.
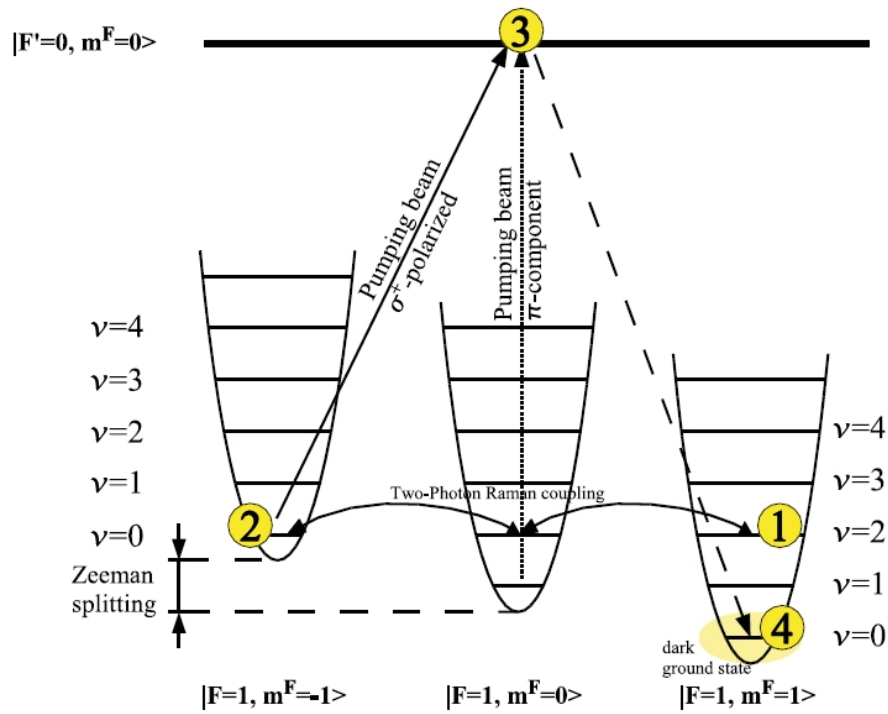
FIGURE 2.1: Degenerate Raman sideband cooling scheme for ^{87}Rb, Atoms starts in $m_F = 1$ state, loses with two photons by Raman transitions and goes to two lower vibrational state, pumped back from $m_F = -1$ and $m_F = 0$ to $m_F = 1$. Atom stays in this cycle till it reaches the vibrational ground state [13].

- Using counter-propagating Raman beams to suppress Doppler shifts. Raman transitions can be induced from the lattice beams as well.

- Atoms reaching the vibrational ground state are stored into a dark state to avoid heating by the resonant scattered photons.

- A weak pump beam recycles atoms and brings them into the cooling cycle.

Chapter 3

Experimental Setup

To perform 3D Raman sideband cooling, a MOT to trap and pre-cool atoms, a far-off-resonant 3D optical lattice and a magnetic field (in order of 50 mG) to tune the vibrational level spacings of the atoms in the optical lattice are needed.

In terms of laser power, $2\times$ diode lasers, working at ^{87}Rb D2 line 780 nm, 40 mW each, will be sufficient for the MOT. For the 3D optical lattice, the Lamb-Dicke regime is satisfied by wavelengths longer than 740 nm, that means 780 nm is a suitable wavelength for the lattice beams. Therefore, another Rb diode laser with minimum power of 60 mW is needed as well.

In addition, atoms are trapped and cooled from a dilute atomic vapor that means a vacuum system with optical access for the MOT and the 3D optical lattice is necessary. The pressure inside the vacuum system defines the collisional loss and therefore the lifetime of the cooling experiment. The lesser the pressure the longer the lifetime of the trapping, for that the vacuum system's desired pressure is in the UHV regime, 10^{-9} mbar and less. UHV regime unlike the other vacuum regimes needs certain care and techniques to reach and can be extremely tricky to troubleshoot. Here the design for a UHV system and its diagnosis and troubleshooting techniques are presented.
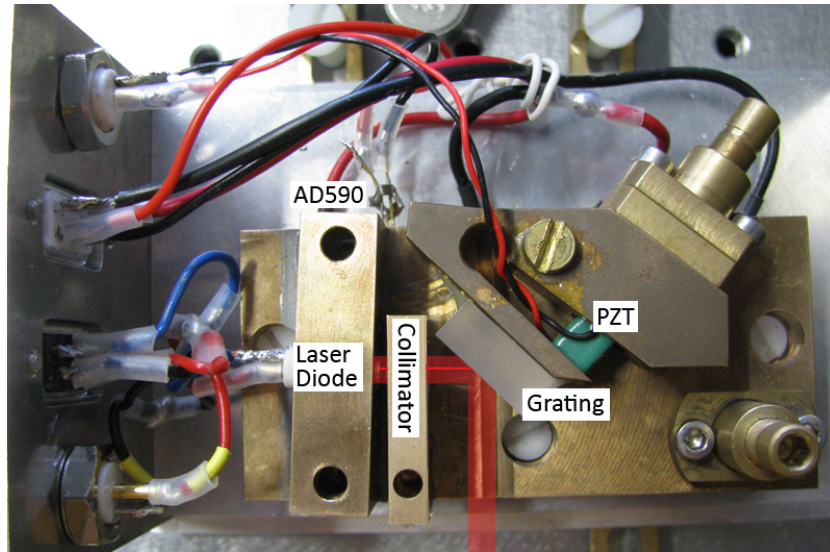
FIGURE 3.1: Laser diode in ECDL setup with Littrow configuration, Optical feedback is shown with the thinner red line.

3.1 Laser System

3.1.1 Diode Lasers

In this setup two different laser diodes have been implemented, Thorlabs DL-7140-201S (785 nm, 70 mW) and Farnell ADL-78901TL (785 nm, 100mW). Laser diodes' outputs depend on their temperature, applied current and optical feedback. Therefore these parameters need controlling to stabilize the laser diode's output. To control the optical feedback, I built the laser diodes into external cavity setups (referred to as ECDL [3, 40]) with gratings in Littrow configuration to provide tunability and frequency locking by controlling the optical feedback from the grating to the laser diode, (see Fig. 3.1).

Temperature control is done by a servo-loop circuit connected to a temperature sensor and Peltier elements as means of cooling. Thermistor and AD590 can be both used as temperature sensor but AD590 has preciser and more accurate readings. The drawback of AD590 is that it suffers from sensitivity to RF noise. Since RF electronics are part of the lab apparatus (e.g. driver electronics for AOMs) to shield AD590 sensors against RF noise, I soldered $3\times$ 10nF SMD capacitors in a triangular setup and close to the sensors' to the pins (Fig. 3.2). Applied current is also controlled by another servo-loop circuit.
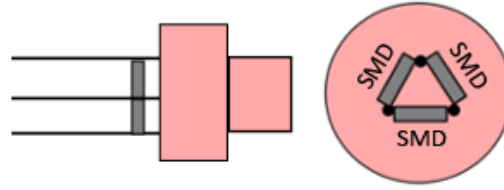
FIGURE 3.2: Shielding an AD590 temperature seonsor against RF noise, 3×
10nF SMD capacitors in a triangular arrangement. Soldering as close as possible
to the can is recommended (on the left).
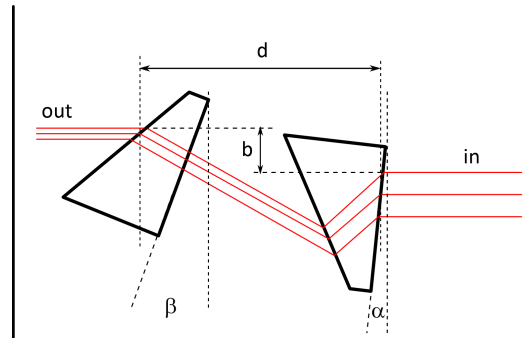

FIGURE 3.3: Alignment of anamorphic prism pair, Stencil for anamorphic prism
pair (Thorlabs PS871-B) with 0.5× magnification, two vertical lines are for
guiding the laser beam (shown in red lines) in the correct angle. $\alpha = 6°$, $\beta =$
$21.1°$, b = 20 mm, d = 5.1 mm

Laser diodes have an elliptical beam, for the MOT in the current apparatus it
does not cause problems but a circular beam can be more efficiently coupled to
an optical fiber and passed through the aperture of a modulator (e.g., AOM). To
circularize the beam *cylindrical lens pairs* or *anamorphic prism pairs* are both
conventional tools.

I used anamorphic prism pairs for their compactness (3 cm in the current setup),
but they are a bit tricky to align because the magnification of anamorphic prism
pairs depends on their relative angle and distance. The incident beam should be
at the Brewster angle (for that they are also called Brewster telescope) but in
case they are aligned carefully they have reasonable efficiency (upto 95%). To
align them I used this easy technique by using stencil. Given their dimensions, I
designed a stencil with the desired angle and distance for the correct magnification
(0.5×), simply placed them on the stencil and they were aligned (Fig. 3.3). The
effect of an anamorphic prism pair on the beam profile is shown in Fig. 3.4.
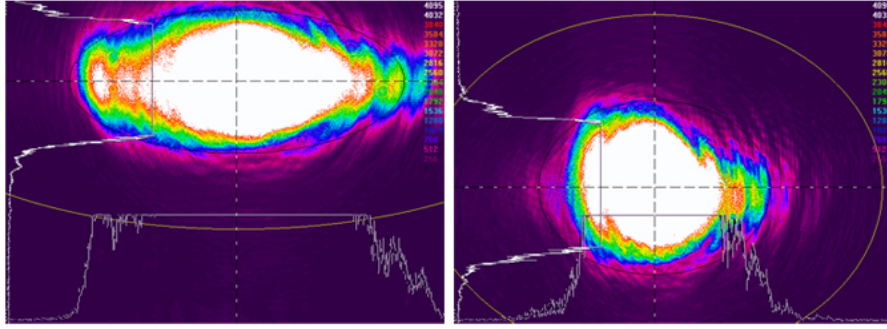
FIGURE 3.4: Beam profile before (left) and after (right) circularization, The picture is saturated but it shows the compressed beam spot. The final beam diameter about 3 mm.

3.1.2 Polarization Spectroscopy

The D2 transition of ^{87}Rb is shown in Fig. 3.5. *Polarization spectroscopy* resolves these transitions. For locking to the transitions, the signal from the polarization spectroscopy is sent to the electronics and then fed back to the piezoelectric stack behind the grating inside the diode laser. The grating moves, changes the optical feedback and this corrects the diode laser's output frequency.

Polarization spectroscopy has been first introduced by Wieman and Hänsch [28, 39] and is based on induced dichroism in a gas sample. Its setup is similar to the saturation spectroscopy but with linearly polarized probe beam and circularly polarized pump beam. Linearly polarized probe beam can be seen as sum of two circularly polarized (σ^+, σ^-) beams. Assuming the pump beam is σ^+, it populates $m_F > 0$ transitions thus the probe beam's σ^+ and σ^- components will experience different absorptions, resulting two different saturation spectra. The difference of these two spectra gives the polarization spectrum. The polarization of the pump beam should be chosen in a fashion that two saturation spectra be of the same amplitude. If so then the difference signal shows the difference induced by the polarization difference not the power difference of the signals.

In the current setup (see Fig. 3.6) probe has been kept at about 50-100 μW and the pump about 0.5-1 mW. To achieve a clear signal with relatively large peaks pump beam should be about 10 times more powerful than the probe beam. A smaller angle between pump and probe beam results better overlapping and therefore improves the signal as well. Typical spectra taken from the spectroscopy setup is shown in Fig. 3.7.
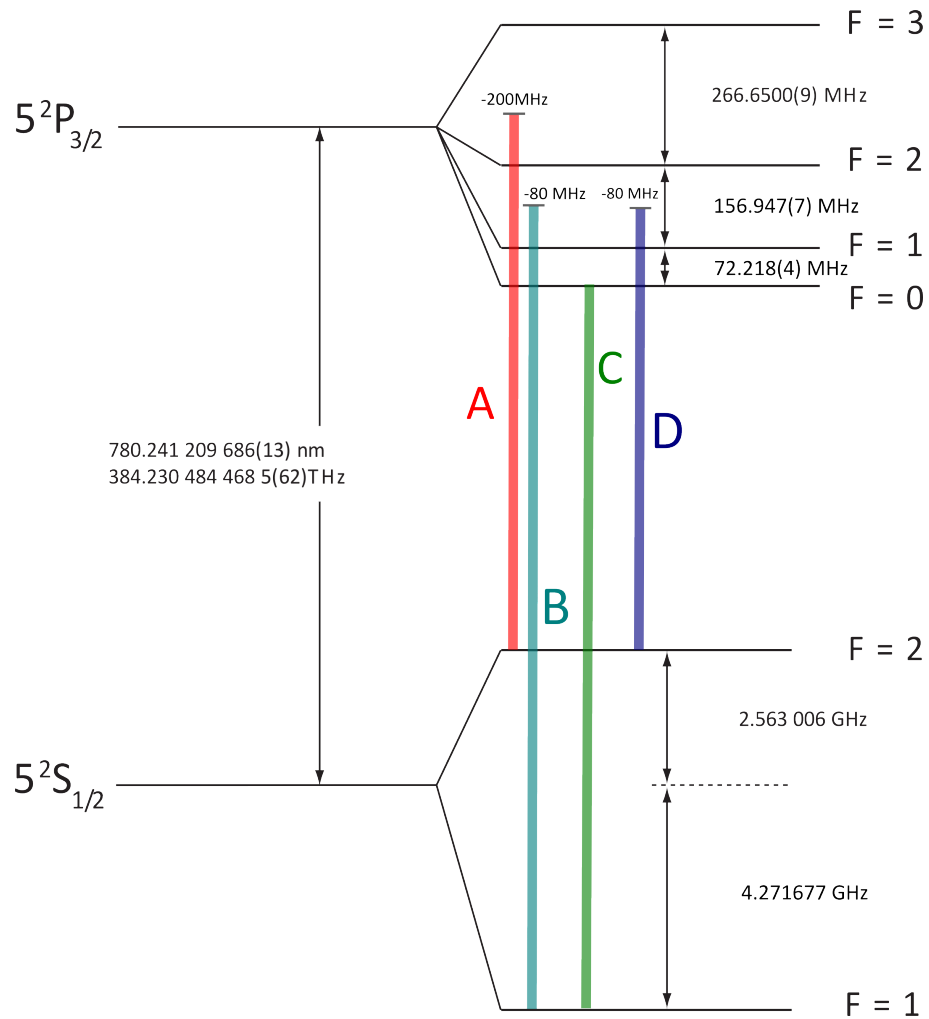
FIGURE 3.5: Transitions of [87]Rubidium D2 line used in the experiment. A: -200 MHz detuned for the MOT, B: -80 MHz detuned for the MOT repumper, C: Raman pump, D: -80 MHz detuned for the optical lattice

The complete laser system setup is shown in 3.8. Two AOMs operating at 80 MHz and 200 MHz have been used in single pass to detune the laser beams for the MOT. Two more AOMs (80 MHz and 130 MHz) are needed for the detuning of the lattice and Raman pumper beams. AOMs are built inside the locking loops since with this method the output power of laser setup does not depend on the AOM's operation and efficiency, therefore I can have more flexible power tuning and use most of the laser power.
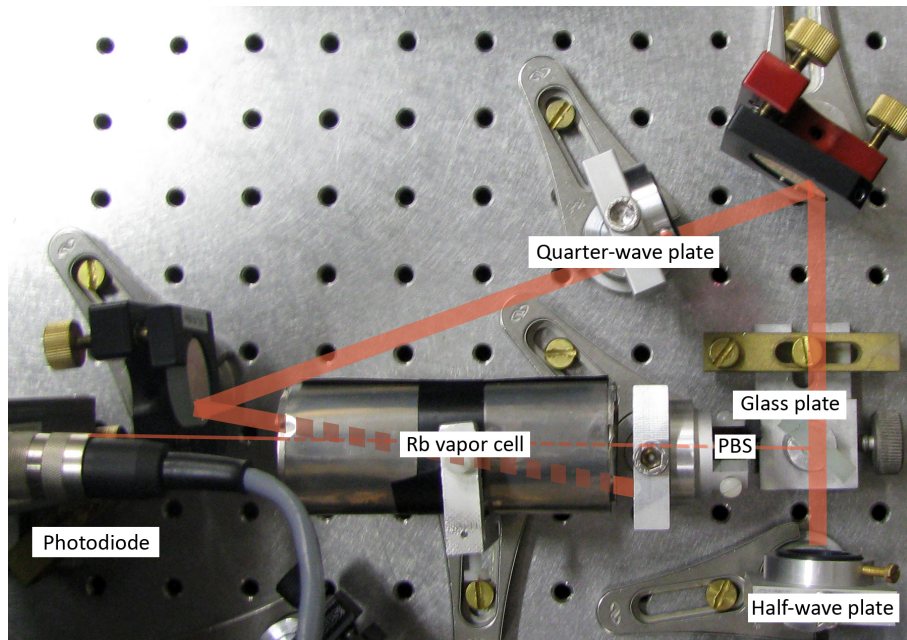
FIGURE 3.6: Polarization spectroscopy setup, the PBS before Rb vapor cell is to ensure linear polarization of the probe beam after reflection from the glass plate.

3.2 Vacuum System

Atomic vapor is the source for atoms in the cooling experiment. But this vapor should be in vacuum since the trapping potential in a MOT or an optical lattice is small in comparison to thermal energies of atoms and most collisions between trapped atoms and the background gas give enough energy to the trapped atom to kick it out of the trap. If the background pressure is too high, atoms are kicked out of the trap faster than they can be loaded, and the trap does not work. This means that the MOT cloud only forms in a vacuum chamber with low atomic vapor pressure. Typical vacuum pressures of less than 10^{-8} mbar are favorable [33]. I have tried to get the lowest pressure possible with the components I had.

3.2.1 Design

The design of the vacuum system is shown in Fig. 3.9. The main chamber is a home-made chamber with 18 view-ports (2× CF150, 2× CF100, 6× CF40 and 8× CF16). This chamber is taken from an old experiment and not all the 18 viewports are needed. 6 viewports for the MOT and 4 viewports for the optical lattice and two left lattice beams share the CF150 viewport with the MOT beams. It is
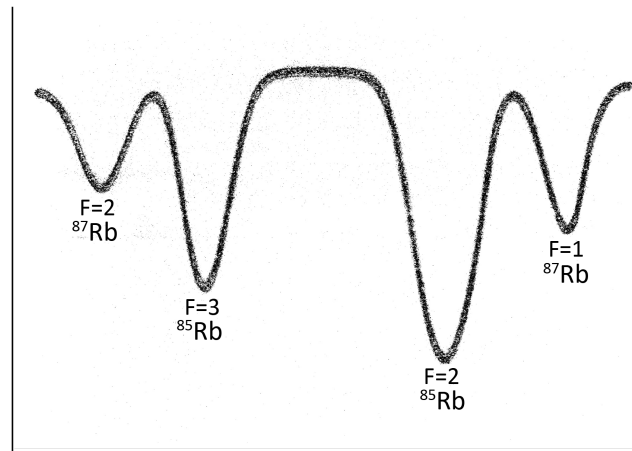
(a) Doppler spectrum
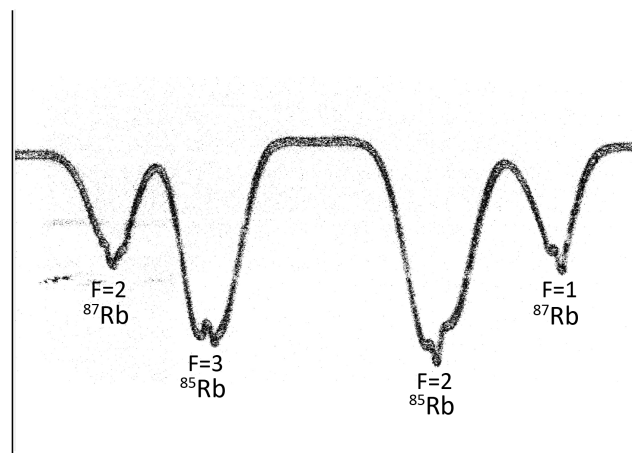
(b) Doppler free saturation spectrum
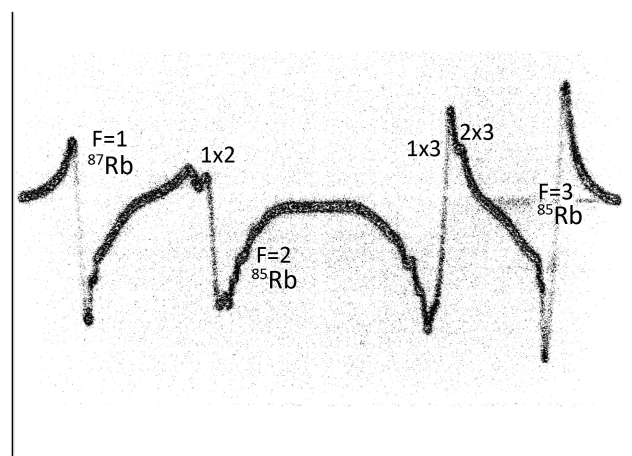
(c) Polarization spectrum

FIGURE 3.7: ^{87}Rb D2 transition spectrum from polarization spectroscopy. Widths and relative heights of the peaks are affected by beam alignment, intensity, and polarization. The quality of images is not good due to the fact they have been taken from the oscilloscopes monitor by a camera. Scale of Y-axis is Volts.

.
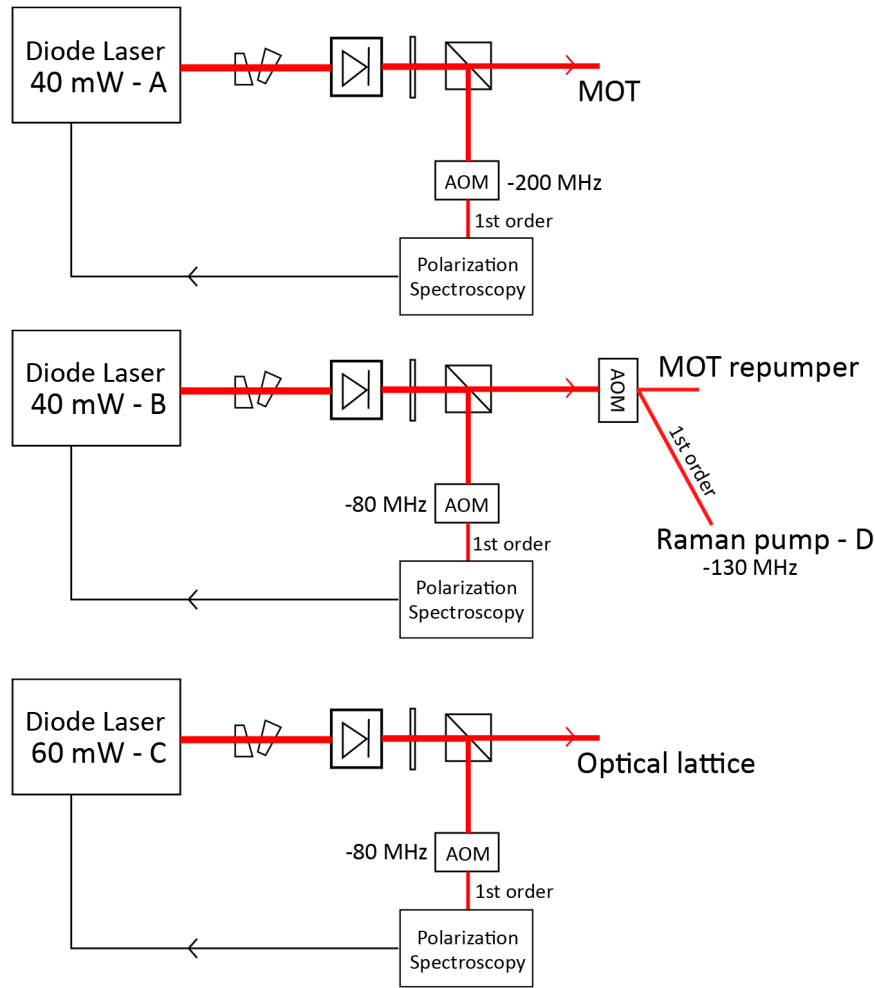
FIGURE 3.8: Complete laser system, Lasers are frequency locked to these transitions: **A** $F = 2 \longrightarrow F' = 3$, **B** $F = 1 \longrightarrow F' = 2$, **C** $F = 1 \longrightarrow F' = 0$, **D** $F = 2 \longrightarrow F' = 2$

connected through a CF100 T component to an ion getter pump (Varian Starcell 150) as the main pump and an oil-free pump station (Pfeiffer TSH-71E) for prepumping. The vacuum system volume is about 100 liters and the ion pump's speed is 125 l.s^{-1}. The pumping scheme has been evacuating using the pump station to 10^{-6} mbar regime and then switching on the ion getter pump for further evacuation since ion getter pump's lifetime is exponentially related to the initial pressure and it can not operate from ambient pressure as shown in the Table. 3.1.

Ion pumps produce a constant stray magnetic field in their surroundings but its present near the pump and it falls quite rapidly[37]. In the current setup the center of the main chamber has been placed at (-300 mm, 120 mm, 120 mm) distance from the center of the ion pump's inlet. that means at the center of the main chamber a constant magnetic field of 0.5 G exists. Pump station is connected

Initial Pressure (mbar)	Life-time (hr)
10^{-3}	20
10^{-4}	200
10^{-5}	2000
10^{-7}	200000 (over 20 yrs)

TABLE 3.1: Typical ion pump lifetime is exponentially related to the initial pump-down pressure [1].
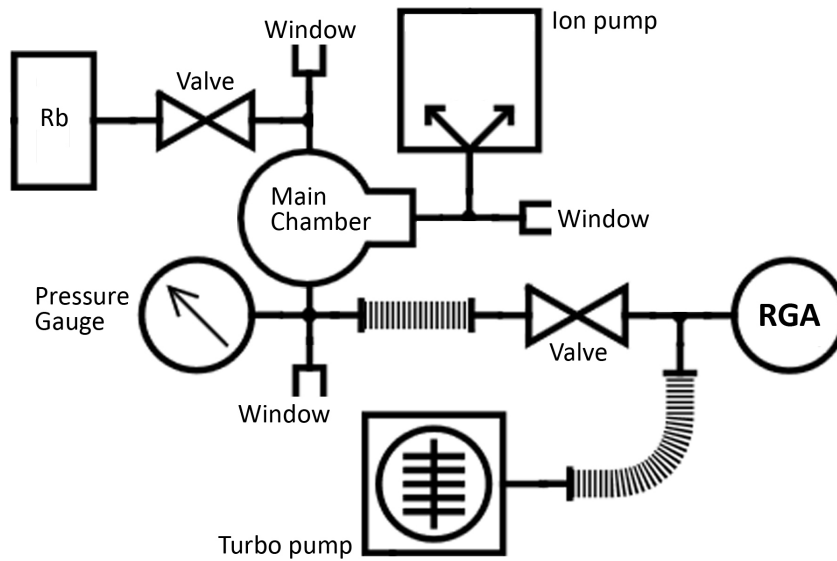
(a) UHV system design, There are 18 viewports on the chamber. Here just those three sharing involving in the design are shown.
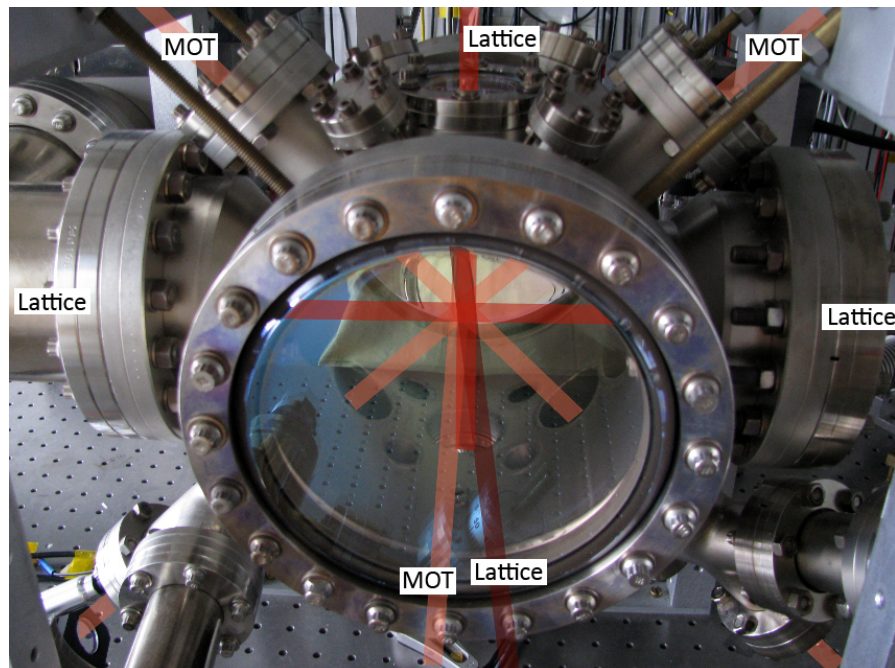
(b) Main chamber and the laser beams, MOT beams and optical lattice beams overlap in the center of the chamber.

FIGURE 3.9: Vacuum system

FIGURE 3.10: A typical feeler gauge, A simple and underrated tool but very helpful in assembling the components to have even tightenings.

after the UHV valve (Varian all-metal valve) through a tube. This tube and the pump station are detached after reaching the desired pressure and the valve is closed forever. The other valve to the Rb reservoir is to control the atomic vapor pressure inside the chamber. RGA module is used for diagnosis and its principle of operation and results are discussed in 3.2.6.

The pressure gauge used in the setup is a Bayard-Alpert ionization gauge (Varian 571) working in the 10^{-3} to 2×10^{-10} range. The final pressure after bake-out and leak tests is 7.1×10^{-10} mbar.

Assembling the vacuum components is time-consuming and needs to be done patiently and carefully. I have tightened the screws and knots in rounds, meaning starting from a screw, tightening a bit and moving on to the other screw, keeping on this procedure (either clockwise or counter-clockwise) till all the screws were tight. The gaps between mating surfaces were checked after each round of tightening with a feeler gauge (Fig. 3.10). Uneven tightening can open up leak. The sealing surface of the all-metal valves and not the bellows should always face the vacuum side, this configuration reduces the surface area in the UHV chamber [25].

Wearing powder-free gloves and working in a clean environment is necessary since grease of a single fingerprint can cause outgassing. Mating knife-edges must be extremely clean and free of any burrs and scratches. Before assembling each component up on the vacuum system I cleaned the knife-edges and the copper gasket with optical tissues and pure acetone for spectroscopy (Uvasol).

3.2.2   Cleaning Process

Exposed surfaces to the vacuum should be free of any substance with considerable vapor pressure and extremely smooth to minimize the microscopic surface and therefore minimizing the amount of adsorbed gas and outgassing [20]. Conventional polishing and buffing is not sufficient and in fact could worsen the outgassing because these processes flatten surface burrs and trap gas underneath [20].

Since the components used to set up this chamber are all taken from the previous experiments they needed to undergo a cleaning process. Different recipes depending on the contaminations and dirts exist [26, 32]. In my case, contaminations were mostly dust, oil, fingerprint grease and oxides. These can be removed by ultrasonic bathing with proper cleaning agent and distilled water.

I grouped the components into aquaphobic, non-aquaphobic and uncleanable components and cleaned them separately. I called valves, feedthroughs, ionization pressure gauges and other complicated components as aquaphobic since they have many nooks and holes which water or cleaning agents can find shelter there, produce outgassing and rust through. Pumps and RGA are uncleanable and for any cleaning process they should be treated by experts.

Aquaphobic components   I mildly cleaned valves, feedthroughs, bellows and ionization gauges in the following recipe and it has been sufficient for the current vacuum system. More intensive cleaning for them should to be done by experts:

1. Bathing in clean acetone for about 30 min.

2. Drying with clean and warm nitrogen.

3. Wrapping in aluminum foil for later use.

Non-aquaphobic components   As cleaning agent I used Tickopur RW77 which is an ammonia based agent and is effective on resinous residues, soot, oil, wax, pigments, silicon oil, oxides of non-ferrous metals. The applied recipe is the following:

1. Bathing in ultrasonic cleaner with a 5% soluton of Tickopur RW77 and distilled water for $10 - 15min$.

2. Bathing in ultrasonic cleaner with distilled water for $10 - 15\,min$ to remove the residual agent.

3. Rinsing with clean acetone (not necessary Uvasol).

4. Drying with clean nitrogen (a warm flow is recommended).

5. Wrapping in clean oil free aluminum foil for later use.

Very dirty components can be treated by bathing for 60 min and then following the steps from 2 to 5. Long cleaning time (60 min) can remove the brownish-golden color (supposedly burnt factory oil [25]) appearing after bake-out on some components.

3.2.3 Pumping Curves and Interpretation

After cleaning and assembling the components, the vacuum system should be tested for reaching the desired pressure. The simplest method is looking at the *pump-down curve* which is pressure fall vs. time during pumping. In an ideal vacuum (clean, tight, without outgassing), pressure fall in time should be exponential [14]. Leaks, outgassing, water vapor and other typical vacuum problems can alter this curve from its so-called *ideal* curve [14].

In (Fig. 3.11) the pump-down curve right after the assembling is shown. Pump-down curve for an ideal system is in fact a straight line(!) in log-log scale and curved pump-down is the sign of leak or outgassing [12].

By looking at the pump-down curve it is not easy to distinguish between leak and outgassing. Since the treatment for each of them is different and takes a tremendous amount of time to test both. Pressure increase in time after turning off the pumps without ventilation (so called *rate-of-rise curve*) can distinguish between leak and outgassing (see Fig. 3.12(b)). Note that a vacuum system can not be literally leak and outgassing free. This depends on the timescale and desired pressure. Even a good vacuum will show increase in pressure by switching off the pumps for long time. To keep the system in the "good" pressure it is needed to either decrease the leak and outgassing rate or increase the pumping speed. It is clear that leaks produce a constant rate in pressure since they are open to an unlimited source of molecules (ambient pressure) and outgassing contribution
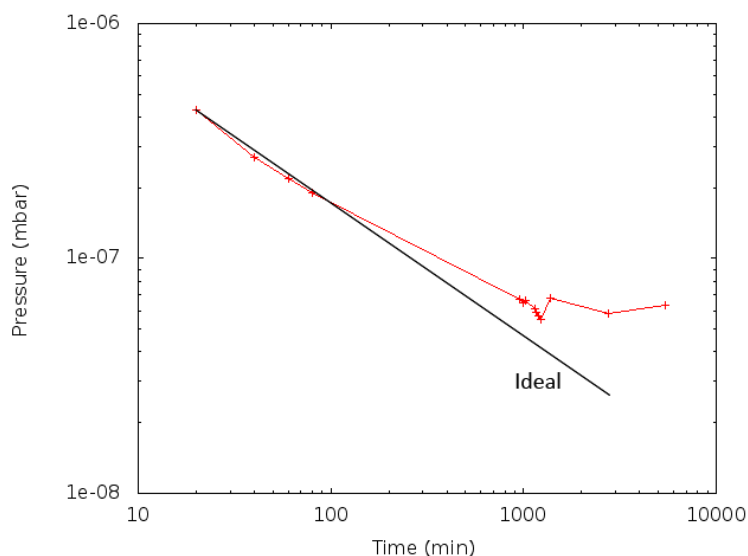
FIGURE 3.11: Pump-down curve, The curved pump-down characterizes a leaky or with outgassing system.

reaches a constant value because its source is a limited amount of some substance inside the vacuum.

Since these readings in Fig. 3.12(b) were taken before bake-out it was obvious that the main contribution to the outgassing comes from water vapor inside. Therefore, for not reaching the desired pressure I baked out the vacuum and performed leak tests after the bake-out.

3.2.4 Bake-out

Water molecules trapped inside the walls of the chamber or sticked to the surfaces (mainly during the cleaning process) come off from the walls gradually and increase the pressure inside the chamber. Water vapor can not be pumped out. Bake-out is the process of increasing the temperature in a vacuum system to remove the water (and organic substances) from the system during pump-down and returning it to the ambient temperature [14]. A typical bake-out should improve the vacuum by one or two order of magnitude [4].

There are very few quantitative information about a typical bake-out cycle [14]. Since water is one of the main reasons for bake-out, leveling the temperature to above 100°C is reasonable. It is well understood that higher temperature and longer bake-out time will result lower pressure but this temperature and bake-out
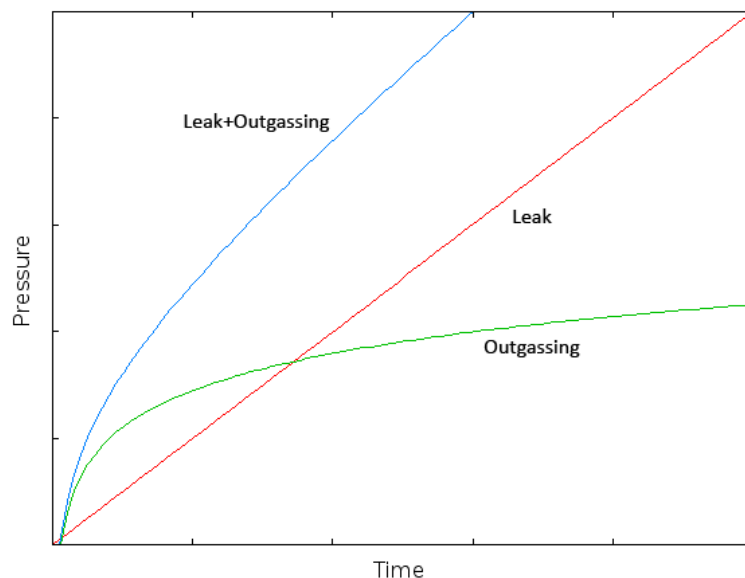
(a) A Typical rate-of-rise curve, comparison between leak and outgassing is shown
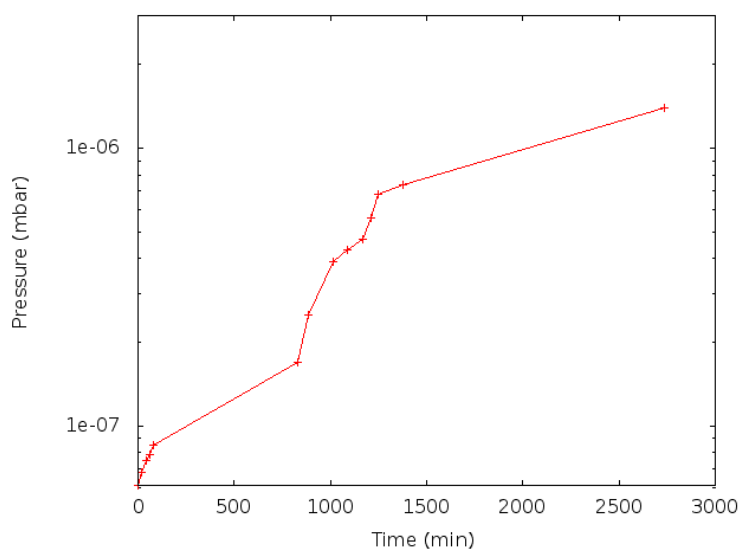
(b) Rate-of-rise curve, Pressure readings taken before bake-out. Comparing to the typical rate-of-rise curve it is clear that leakage and outgassing are both present.

time are limited by the vacuum components used in the system [4]. To remove organic substances baking to 400 C is recommended but in that case special gaskets must be used and all components must be checked if they are bake-able to that high temperature.

During bake-out a uniform temperature gradient in the vacuum system is necessary since large temperature gradients can produce tension in the components and open pores on the connections. Besides, there should be special care taken for glass-metal transitions. Because glass and metal they have different thermal expansion

ratios. For that I tried to keep the temperature gradient below 10 °C.cm^{-1}.

The whole vacuum system (except the pump station) was wrapped in heating tapes in a fashion that tapes did not cross each other and windings had somewhat equal gaps in between. For a better heat conduction (since stainless steel has poor heat conduction) I covered all the surfaces with 2-3 fold layers of aluminum foil and placed temperature sensors all over the system and on the critical positions (e.g. glass-metal transitions on the large windows). Temperature has been leveled gradually and monitored during process. Temperature has been balanced by tuning the applied voltage or adding adding removing aluminum foils.

The current system has been baked-out three times. Leaks and a malfunctioning pressure gauge were the reasons for this. Readings of the two last bake-outs are discussed here (the first bake-out had no accurate pressure readings). The maximum temperature has been increased to above 150°C and below 200°C since there were concerns about the bake-ability of large windows (CF150) to higher than 250°C.

Pressure readings are shown in Fig 3.12. There are two peaks clearly observable in both reading. I guess they are coming from the difference between *adsorption* and *absorption* of water in the walls of the system. First peak is for the adsorbed (water sticked to the surface) and second one absorbed water (water trapped in the depth of steel).

Overall, it seems for a vacuum system of about 70-100 liters (current setup), 60 hrs of baking is sufficient but there is no certain rule for that, the best way is to monitor the pressure inside and stop baking when no significant rise in pressure is observable. As mentioned before if the components and gaskets are bake-able at higher temperature always leveling to higher temperature is recommended.

For cooling down and bringing the system to the ambient temperature, again I decreased the temperature gradually in 15-20 hrs and tried to kept the main chamber at higher temperature (+50°C) comparing to the pumping part since colder regions are more attractive for the gas inside, this produced a water vapor flow towards the pump.
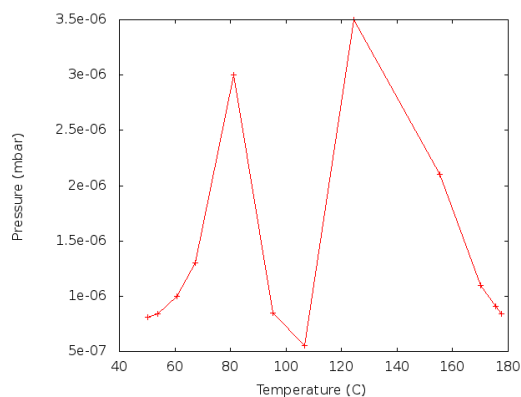
(c) 2nd Bake-out: Pressure vs. Temperature
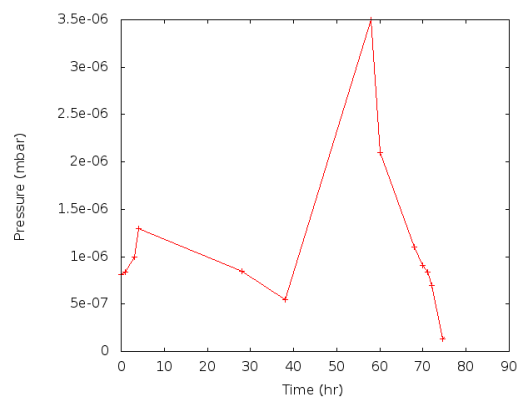
(d) 2nd Bake-out: Pressure vs. Time
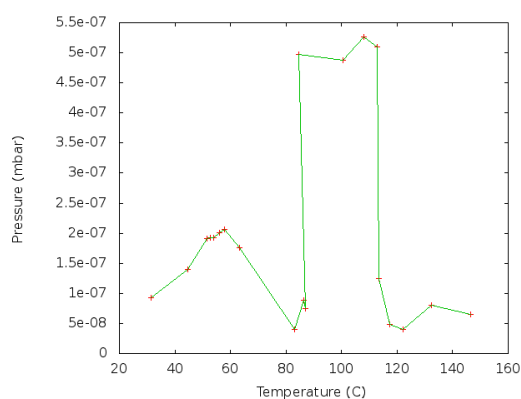
(e) 3rd Bake-out: Pressure vs. Temperature
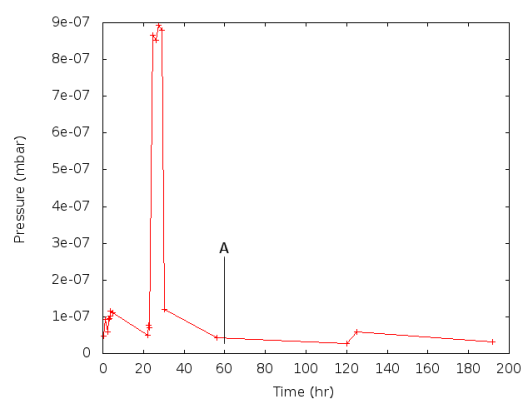
(f) 3rd Bake-out: Pressure vs. Time, After the mark **A** baking did not improve the pressure significantly.

FIGURE 3.12: Pressure evolution during bake-out cycle, Two pressure peaks are visible in both measurements

3.2.5 Leak Test

After the first bake-out, by looking at the pump-down curve existence of leaks in the vacuum been confirmed. As a crude test I used drops of clean acetone on the flanges, weldings and looked for dramatic changes in pressure. Basically in presence of a leak, a rise in pressure is expected by dropping the acetone on the suspicious region but I observed a reproducible short-time pressure fall. I guess if the leak is close enough to the pump comparing to the pressure gauge a short pressure fall is possible due to the fact that acetone can seal the leak for a short period of time but when it enters the system it is pumped out before reaching the pressure gauge.

The acetone test can detect very small leaks (roughly below 10^{-6} mbar.l.s^{-1}). The ultimate test is using *Helium leak detectors* [41].
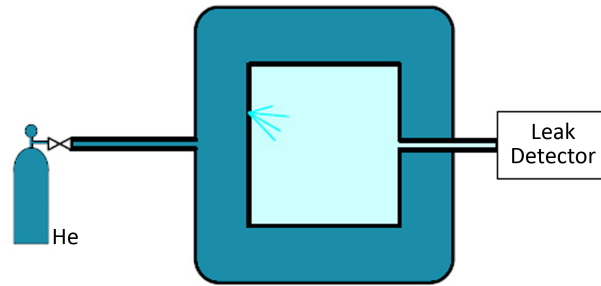
(a) Total leak test, can be used to approximately locate the leak. Dark colored box is the covering (plastic bag).
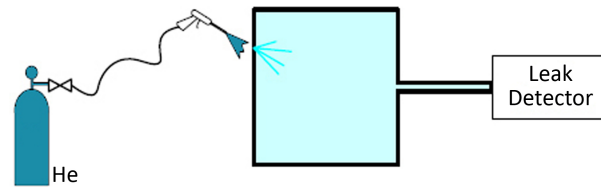
(b) Tracer leak test, used to locate the exact position of the leak

FIGURE 3.13: Helium leak test techniques, The light colored boxes are the vacuum system [41].

Helium has been used for the first time for leak detection in Manhattan project [18] and has some advantages over other gases. It is non-toxic, chemically inert, inexpensive to produce and is a small and light molecule and can easily penetrate through small leaks besides it is present in small quantity in atmosphere (5 ppm [30]) thus can not be naturally present inside vacuum before leak test. Therefore an increase in helium pressure is the sign for a leak [18, 41]. Ionization pressure gauges are not sensitive enough to detect this short-time small increases in pressure. Therefore a leak detector is needed. Leak detector is basically a mass spectrometer that looks for Helium inside the vacuum. I have used a residual gas analyzer which can do this task. The details about its spectra comes is the next section 3.2.6.

I did the Helium leak test in two methods shown Fig. 3.13. **Total leak test**, which is done by grouping components, covering them together with a plastic bag and filling the bag with Helium. By this method I could locate the approximate position of the leak and save time. **Tracer leak test**, After total leak test, I made a simple Helium nozzle with the needle of a syringe and tested all the weldings, connections and glass-metal transitions and for more inspection. Helium leak test showed some few very small leaks at 10^{-11} mbar but nothing significant.
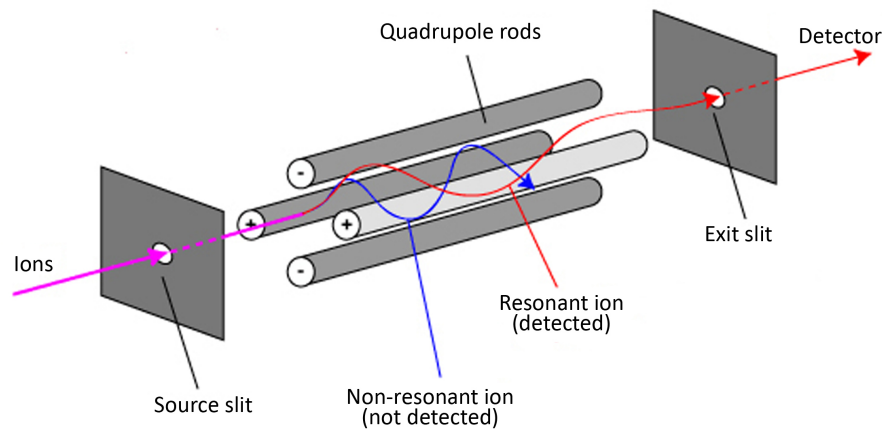
FIGURE 3.14: Quadrupole mass spectrometer principle, The ions can travel through the rods and reach the detectors only for some certain values of the applied potential on the rods [15].

3.2.6 Diagnosis using Residual Gas Analyzer

Residual Gas Analyzer (RGA) is a rugged mass spectrometer based on electric quadrupoles, designed to monitor the contaminations in vacuum systems and perform leak tests. I used VACSCAN 1 RGA module from LEDA-MASS for this purpose.

Quadrupole mass spectrometer consists of four cylindrical or hyperbolic rods in a square configuration. Opposite rod pairs have the same potential which has a DC and an AC component (in RF range) shown in the Fig. 3.14.

Gas sample is ionized by passing through filaments and by an attractive force exerted on it from one of the rods with the opposite charge enters the quadrupole assembly [15]. For each *mass/charge* ratio there is a certain set of choices of DC and AC voltage that satisfies the equations of motions and let the ion pass through rods without hitting them. The successful ions are detected at the end of the rods and by measuring their charges using *Faraday cup* or *electron multiplier* (shown in Fig. 3.15) their mass is determined. VACSCAN 1 has both Faraday cup and electron multiplier detectors. Faraday cups is not as sensitive as electron multiplier detector but it works better in higher pressures (namely above 10^{-8} mbar for low pressures electron multiplier is favorable.

The mass spectrum of the vacuum given by RGA characterize the system. The typical spectrum is partial pressure vs. mass therefore it shows what substance is contributing to the total pressure. In Fig. 3.16 the spectrum of the current system

(a) Faraday cup, An ion hitting the cup is neutralized and this produces a small current.

(b) Electron multiplier, An ion hitting electrode causes secondary emissions.
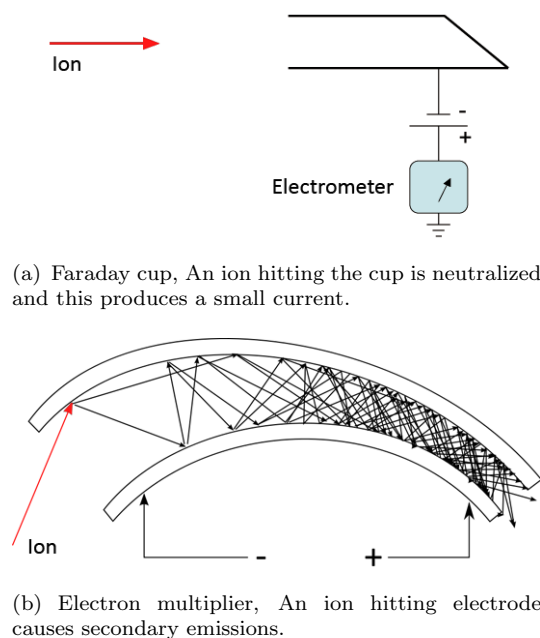
FIGURE 3.15: Typical charge detectors used in quadrupole mass spectrometers. Electron multiplier can get saturated in pressures higher than 10^{-8} mbar.
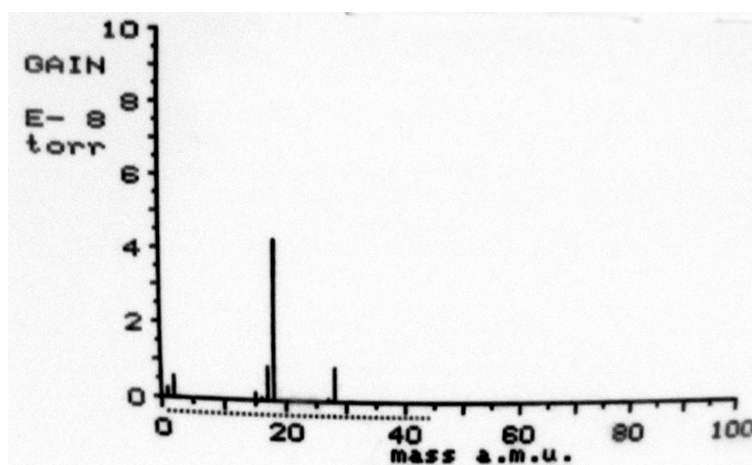

FIGURE 3.16: Mass spectrum of the vacuum system before bake-out, Water peaks at 17 a.m.u for hydroxyl and 18 for water vapor are significant.

before bake-out is shown. Hydroxyl (OH⁻) comes from broken water molecules. Fig. 3.17 shows the system right after the bake-out and starting to cool-down, water has been pumped out of the system.

The proof for the leakage in the system using the mass spectrum is also possible. An air leak produces a fingerprint like Fig. 3.18. Peaks at 14 and 28 for Nitrogen, 16 and 32 for Oxygen and 40 for Argon which is expectable since atmosphere composed of 78% N_2, 21% O_2 and about 0.9% Ar [30].
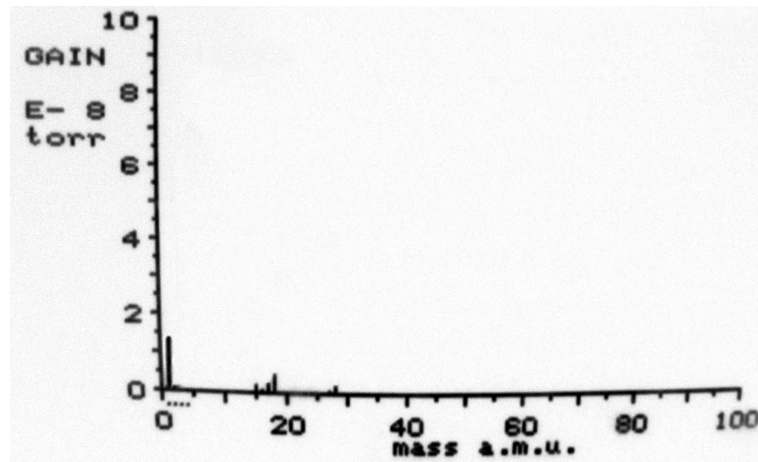
FIGURE 3.17: Mass spectrum of the vacuum system after bake-out, Water peaks are vanished.
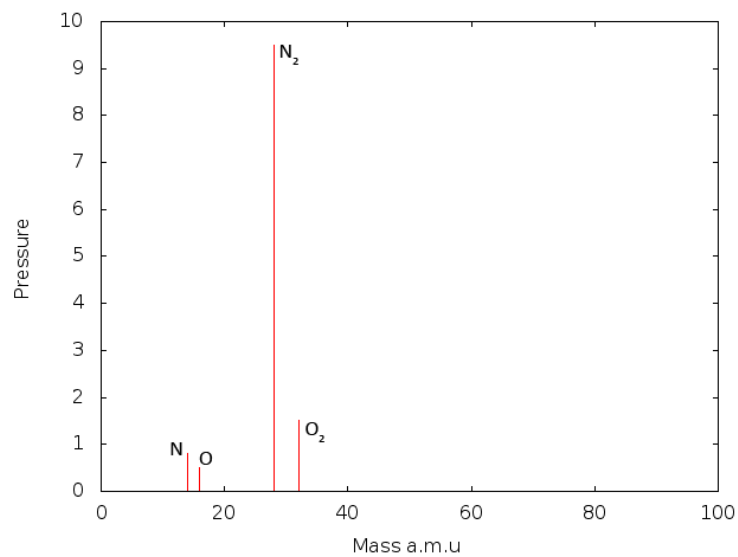
FIGURE 3.18: Fingerprint of an air leak [23]

Another common problem in a vacuum system which is also observable in Fig. 3.16 is the presence of Carbon monoxide and dioxide, Peaks at 28 for CO and 44 for CO_2 characterize this problem. The teatment is degassing all the filaments (RGA, ionization pressure gauges, ...) and high temperature bake-out if degassing is not effective 3.2.4.

Chapter 4

Conclusions and Outlook

4.1 Current State of the Apparatus

In this text Degenerate Raman sideband cooling as a method to pass the recoil limit and provide a colder sample for evaporative cooling in the process of reaching BEC has been introduced.

The design for a laser system based on three diode lasers for a MOT to trap and pre-cool the atoms and the 3D optical lattice to perform the degenerate Raman sideband cooling is presented. Three external cavity diode lasers working at $780nm$ with 40 mW and 60 mW of power are built and locked to ^{87}Rb D2-line using polarization spectroscopy.

In addition, A UHV system with the final pressure of 7.1×10^{-10} is built. Reaching a UHV regime has lots of difficulties and needs certain techniques and care. Here the techniques I have sued to maintain such low pressure, namely: cleaning recipe, pump down, bake-out and leak tests has been discussed in details.

4.2 Future Work

After getting the MOT run, 3D optical lattice and cooling scheme can be set up by following the experiments done in [13, 29] the cooling setup will be an optical lattice formed by interference of four linearly polarized laser beams (see Fig. 4.1), two counter-propagating along the x axis, and two running waves along y and
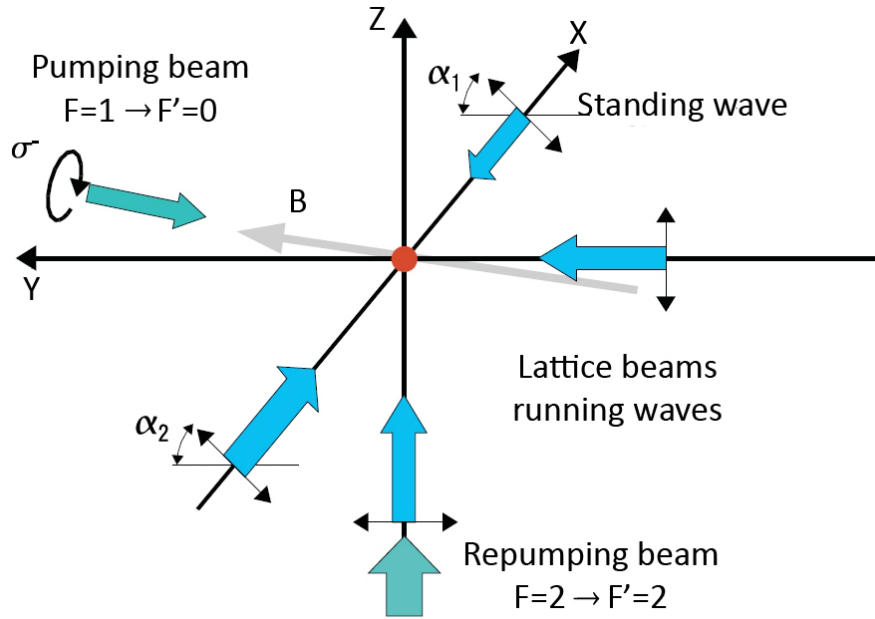
FIGURE 4.1: Laser beams setup for the 3D Raman sideband cooling, following the setup by Treutelin [29] and Fölling [13]. Two running waves and two counter propagating beams form the lattice. This configuration is more stable than 6 counterpropagating beams. All beams are polarized in the y-z plane to maximize Raman coupling for a magnetic field in that plane. [13].

z. A 6-beam lattice looks like the trivial choice but sub-wavelength movements of mirrors caused by a small vibration could change the relative phase of the standing waves and destroy the lattice. In 1993 it has been shown [38] that for an n-dimensional lattice, $n + 1$ traveling waves are sufficient and using this scheme lattice geometry is unchanged by fluctuations in the relative phases of the beams apart from an overall translation of the lattice [38]. The polarizations of the beams are all in the y-z plane to maximize the Raman coupling for a magnetic field in that plane. The polarizations of the counter-propagating beams have subtend angles (α_1 and α_2) of typically 30° and 15° [29] or $\mp 10°$ with respect to the y axis.

The detuning of the lattice is in order of $10\,GHz$ [2, 29] to the red of ^{87}Rb D2 line. As mentioned before, detuning (typically $6.8\,GHz$) can be chosen such that the lattice beams also provide hyperfine repumping light to recycle atoms that are pumped into $F = 2$ ground state and eliminate the need for a separate pump beam [29]. The beam that is used to pump atoms into the $F = 0$ state propagates along y and needs power in order of μW. In order to have the weak π and the strong σ^+ components in the polarization along the magnetic field B, B is oriented in the x-y plane at a small angle ($\sim$ 5°) of 5° with respect to y and adjust the polarization of the pumping beam to eliminate the σ^- component. B field is

usually in order of mG. The beam along z can be typically 3 times stronger than those along x and y [2]. The intensity ratios between the beams and the angles α_1 and α_2 can be optimized to obtain low temperatures in all three dimensions. [2, 29]

Bibliography

[1] *Basic Vacuum Practice*. Agilent Technologies (Varian Inc).

[2] Cheng Chin Andrew J. Kerman, Vladan Vuletic and Steven Chu. Beyond optical molasses: 3d raman sideband cooling of atomic cesium to high phase-space density. *Phys. Rev. Lett.*, 84, 2000.

[3] A. S. Arnold, J. S. Wilson, and M. G. Boshier. A simple extended-cavity diode laser. *Review of Scientific Instruments*, 69(3):1236–1239, March 1998. URL http://link.aip.org/link/?RSI/69/1236/1.

[4] C. K. Sinclair B. M. Dunham. Evacuation and bakeout of the illinois/cebaf polarized electron source after minor changes. Technical report, Nuclear physics lab, university of illinois at urbana champagin, 1990.

[5] C.J. Myatt C.S. Wood D. Leibfried D. Kielpinski W.M. Itano C. Monroe B.E. King, Q.A. Turchette and D.J. Wineland. *From Microscopic Towards Mesoscopic: Quantum State Engineering with Cold Trapped Ions*, chapter Mesoscopic and Macroscopic Quantum Phenomena. Nova Science, 2003.

[6] Robert W. Boyd. *Nonlinear optics*. Academic Press, 2008.

[7] J.J. Tollett C.C. Bradley, C.A. Sackett and R.G. Hulet. Evidence of bose-einstein condensation in an atomic gas with attractive interactions. *Phys. Rev. Lett.*, 75:1687–1690, 1995.

[8] Henrik Smith Christopher Pethick. *Bose-Einstein condensation in dilute gases*. Cambridge University Press, 2002.

[9] EA Cornell and CE Wieman. Nobel Lecture: Bose-Einstein condensation in a dilute gas, the first 70 years and some recent experiments. *REVIEWS OF MODERN PHYSICS*, 74(3):875–893, JUL 2002. ISSN 0034-6861.

[10] J. Dalibard D. J. Wineland and C. Cohen-Tannoudji. Sisyphus cooling of a bound atom. *J. Opt. Soc. Am. B*, 9, 1992.

[11] J. Dalibard and C. Cohen-Tannoudji. Laser cooling below the Doppler limit by polarization gradients: simple theoretical models. *J. Opt. Soc. Am. B*, 6 (11):2023–2045, November 1989. doi: 10.1364/JOSAB.6.002023. URL http://dx.doi.org/10.1364/JOSAB.6.002023.

[12] Phil Danielson. The vacuum lab. URL http://www.vacuumlab.com/.

[13] Simon Foelling. 3d raman sideband cooling of rubidium. Master's thesis, Faculty of Physics and Astronomy, University of Heidelberg, 2003.

[14] Robert Warner Carlson G. L. Weissler. *Vacuum physics and technology*. Academic Press Inc., 1979.

[15] Jrgen H. Gross. *Mass Spectrometry*. Spring, 2204.

[16] S. E. Hamann, D. L. Haycock, G. Klose, P. H. Pax, I. H. Deutsch, and P. S. Jessen. Resolved-sideband raman cooling to the ground state of an optical lattice. *Phys. Rev. Lett.*, 80(19):4149–4152, May 1998. doi: 10.1103/PhysRevLett.80.4149.

[17] Peter Van der Straten Harold J. Metcalf. *Laser cooling and trapping*. Springer, 1999.

[18] N. Hilleret. Leak detection. Technical report, CERN, Geneva, Switzerland.

[19] P.S. Jessen and I.H. Deutsch. Optical lattices. volume 37 of *Advances In Atomic, Molecular, and Optical Physics*, pages 95 – 138. Academic Press, 1996. doi: DOI:10.1016/S1049-250X(08)60099-3. URL http://www.sciencedirect.com/science/article/B8JD4-4S8V85B-6/2/bf66905e2bd1deedb43ba4da8955089e.

[20] Michael A. Coplan John H. Moore, Christopher C. Davis. *Building scientific apparatus: a practical guide to design and construction*. Westview Press, 2002.

[21] M. Andrews M. van Druten D. Durfee D. Kurn K. Davis, M-O. Mewes and W. Ketterle. Bose-einstein condensation in a gas of sodium atoms. *Phys. Rev. Lett.*, 75, 1995.

[22] Wolfgang Ketterle and N.J. Van Druten. Evaporative cooling of trapped atoms. volume 37 of *Advances In Atomic, Molecular, and Optical Physics*, pages 181 – 236. Academic Press, 1996. doi: DOI:10.1016/ S1049-250X(08)60101-9. URL http://www.sciencedirect.com/science/ article/B8JD4-4S8V85B-8/2/d579cfa130b944ea0f9338ea54406f4d.

[23] *LEDAMASS VACSCAN 1*. LEDA-MASS Ltd., 1990.

[24] S. Stringari Lev Petrovich Pitaevski. *Bose-Einstein condensation*. Oxford University Press, 2003.

[25] Heather Jean Lewandowski. *Coherences and correlations in an ultracold Bose gas*. PhD thesis, Faculty of the Graduate School of the University of Colorado, 2002.

[26] Keith Middleman. Cleaning for uhv/xhv at daresbury laboratory. Technical report, ASTeC Vacuum Science Group, STFC Daresbury Laboratory.

[27] C. Monroe, D. M. Meekhof, B. E. King, S. R. Jefferts, W. M. Itano, D. J. Wineland, and P. Gould. Resolved-sideband raman cooling of a bound atom to the 3d zero-point energy. *Phys. Rev. Lett.*, 75(22):4011–4014, Nov 1995. doi: 10.1103/PhysRevLett.75.4011.

[28] C P Pearman, C S Adams, S G Cox, P F Griffin, D A Smith, and I G Hughes. Polarization spectroscopy of a closed atomic transition: applications to laser frequency locking. *Journal of Physics B: Atomic, Molecular and Optical Physics*, 35(24):5141, 2002. URL http://stacks.iop.org/0953-4075/ 35/i=24/a=315.

[29] Keng Yeow Chung Philipp Treutlein and Steven Chu. High-brightness atom source for atomic fountains. *Phys. Rev. A*, 63, 2001.

[30] M. Pidwirny. *Fundamentals of Physical Geography*. 2006. URL http://www. physicalgeography.net/fundamentals/7a.html.

[31] E. L. Raab, M. Prentiss, Alex Cable, Steven Chu, and D. E. Pritchard. Trapping of neutral sodium atoms with radiation pressure. *Phys. Rev. Lett.*, 59 (23):2631–2634, Dec 1987. doi: 10.1103/PhysRevLett.59.2631.

[32] L. Schulz. Vacuum component cleaning procedure. Technical report, Paul Scherrer Institut, 2002.

[33] David E. Sproles. Laser spectroscopy and magneto-optical trapping of rubidium atoms. Master's thesis, Stony Brook University, 2008.

[34] Steven J. Oliver Steffen Wolf and David S. Weiss. Suppression of recoil heating by an optical lattice. *Phys. Rev. Lett.*, 85, 2000.

[35] A. V. Taichenachev, A. M. Tumaikin, V. I. Yudin, and L. Hollberg. Two-dimensional sideband raman cooling and zeeman-state preparation in an optical lattice. *Phys. Rev. A*, 63(3):033402, Feb 2001. doi: 10.1103/PhysRevA. 63.033402.

[36] Peter van der Straten and Harold Metcalf. The quest for bec. September 2002.

[37] *VacIon Plus 150 pumps*. Varian Technologies.

[38] P. Verkerk, D. R. Meacher, A. B. Coates, J.-Y. Courtois, S. Guibal, B. Lounis, C. Salomon, and G. Grynberg. Designing optical lattices: An investigation with cesium atoms. *EPL (Europhysics Letters)*, 26(3):171, 1994. URL http://stacks.iop.org/0295-5075/26/i=3/a=003.

[39] C. Wieman and T. W. Hänsch. Doppler-free laser polarization spectroscopy. *Phys. Rev. Lett.*, 36(20):1170–1173, May 1976. doi: 10.1103/PhysRevLett.36. 1170.

[40] Carl E. Wieman and Leo Hollberg. Using diode lasers for atomic physics. *Review of Scientific Instruments*, 62(1):1–20, January 1991. URL http://link.aip.org/link/?RSI/62/1/1.

[41] K. Zapfe. Leak detection. Technical report, Deutsches Elektronen-Synchrotron DESY, Hamburg, Germany, 2007.